Hindawi
Scientific Programming
Volume 2022, Article ID 7140673, 7 pages
https://doi.org/10.1155/2022/7140673

Research Article

Improved Algorithm-Based Magnetic Resonance Images Combined with Computed Tomography in the Diagnosis of Acquired Immune Deficiency Syndrome Combined with Spinal Tuberculosis

Chengming Jiang,[1] **Lin Jiang**,[1] **Langtao Shi**,[1] **and Sainan Jiang**[2]

[1]*Department of Spine Surgery, The First Hospital of Changsha, Changsha 410005, Hunan, China*
[2]*Department of Science and Education, The First Hospital of Changsha, Changsha 410005, Hunan, China*

Correspondence should be addressed to Sainan Jiang; 201711004218@stu.zjsru.edu.cn

Received 15 October 2021; Revised 12 January 2022; Accepted 17 January 2022; Published 9 March 2022

Academic Editor: M. Pallikonda Rajasekaran

This study aimed to analyze the diagnostic value of magnetic resonance imaging (MRI) combined with computed tomography (CT) based on the improved algorithm for acquired immune deficiency syndrome (AIDS) combined with spinal tuberculosis, so as to provide an effective reference theory for the clinical application of imaging diagnosis. The ResNet and Inception network structure were combined to form an improved convolutional neural grid classification (CNGC) algorithm. The improved algorithm was applied to AIDS patients with spinal tuberculosis to evaluate its diagnostic effect and value. 50 patients with AIDS and spinal tuberculosis and 50 patients with spinal tumors were selected for MRI and CT scans. The results showed that the accuracy, specificity, and sensitivity of the improved ResNet-Inception algorithm were much higher than those of the ResNet18 and GoogLeNet algorithms. In addition, compared with the training losses of ResNet18 and GoogLeNet algorithms that converged after 700 times, the ResNet-Inception algorithm only required 350 times to achieve convergence. Based on the improved ResNet-Inception algorithm, the false positive rate (FPR) of AIDS combined with spinal tuberculosis in imaging examinations was about 4%, which was greatly lower than that of the other two traditional algorithms ($P < 0.05$). It can be seen that the improved ResNet-Inception algorithm was more valuable than traditional algorithms for MRI combined with CT in the diagnosis of AIDS combined with spinal tuberculosis and showed great clinical value for the diagnosis of the disease and the differential diagnosis of spinal tumors.

1. Introduction

Acquired immune deficiency syndrome (AIDS) is caused by human immunodeficiency virus infection and belongs to the immune system deficiency syndrome dominated by T-cell immunodeficiency [1, 2]. The immune system of AIDS patients is low, and they are very likely to be infected with other diseases [3, 4]. Tuberculosis is the most common and most likely secondary infection, and it is also one of the longest causes of death of AIDS patients [5]. Therefore, in recent years, the number of AIDS patients with spinal tuberculosis has gradually increased, and the corresponding diagnosis and treatment methods are different from single disease infection, and the main characteristics of the two diseases need to be considered [6–9]. Patients with combined disease mainly manifested as combined lung and extrapulmonary tuberculosis. Among them, a large group of patients with extrapulmonary tuberculosis manifested as spinal tuberculosis [10–13].

There are two main types of diagnostic methods for AIDS combined with spinal tuberculosis: laboratory tests and imaging tests. Laboratory examinations often use polymerase chain reaction technology, recombinant enzyme polymerase isothermal amplification technology, and

GeneXpert detection technology, to achieve the purpose of diagnosis of diseases through the rapid amplification of nucleic acids [14]. In addition, the increase in blood cell sedimentation rate and C-reactive protein are often used as laboratory diagnostic methods, but this type of diagnostic technology has a major drawback. The test indicators are nonspecific, and there is often the possibility of misdiagnosing other spinal-related tumors or infections as AIDS combined with spinal tuberculosis [15, 16]. At the same time, this diagnosis result cannot identify the specific reasons for the changes in the indicators. Therefore, it is of little significance in the diagnosis of AIDS patients with spinal tuberculosis. There are several types of imaging examinations: magnetic resonance imaging (MRI), computed tomography (CT), and X-ray photography, etc. [17]. Among them, X-ray photography has great advantages in imaging examinations. It is characterized by the low cost of detection and easy operation of the detection process. A more comprehensive assessment can also be carried out. At the same time, it is clear whether there are other diseases such as spinal fracture deformity or degenerative changes. Its disadvantage is that it is diagnosed in the middle or late stage of the disease, and it is unable to provide guiding opinions for the early diagnosis [18]. Compared with X-ray photography, CT has great advantages in early diagnosis and higher sensitivity and can avoid the influence of overlap or artifacts in the X-ray photography process. In addition, CT can show the specific conditions of bone disease in more detail and perfection [19]. MRI is superior to CT in early diagnosis. For the inspection and diagnosis of spinal calcification, abnormal pyramidal shape, and destruction of intervertebral discs, MRI is more sensitive and has a higher detection rate [20]. For a more comprehensive and accurate diagnosis and examination of AIDS patients with spinal tuberculosis, it is more common to use a combination of these three detection methods or a combination of two.

Clinicians often cannot sum up quantitative and accurate medical information from MRI or CT images with the naked eye. The emergence of medical image analysis and processing technology has solved this dilemma and has become an important helper for clinical diagnosis. By reading a large number of extremely complex impact information from MRI or CT detection results, and establishing corresponding algorithms for further analysis and clarification, it helps clinicians to diagnose the disease more accurately and quickly and obtains more in-depth information about the disease. However, MR or image contrast is low, and each organization in the image is not clearly distinguished. Traditional image processing methods cannot accurately segment and extract clear and intuitive edges and obtain accurate edge data information. Convolutional neural network (CNN) is a type of deep neural network. The component is a deeper grid structure, which can read image data as visible pathological features and discover feature data that cannot be read by the human eye. This is very important for MRI and CT images in the diagnosis of AIDS with spinal tuberculosis [21–24]. It is worthy of further exploration and pursuit to optimize and improve it to show the shape and pathological changes of the spine more clearly.

In this study, the ResNet was combined with Inception network structures and introduced with the stem, SE-block, and reduction to form an improved convolutional neural grid classification (CNGC) algorithm, which was applied to patients with AIDS combined with spinal tuberculosis and compared with the traditional ResNet18 and GoogLeNet to evaluate its diagnostic effect and value. 50 AIDS patients with spinal tuberculosis and 50 cases of spinal tumors were selected, and they were scanned by MRI and CT; different classification algorithms were used to compare the diagnostic effects of AIDS combined with spinal tuberculosis to evaluate the diagnostic value of MRI combined with CT based on the improved algorithm.

2. Materials and Methods

2.1. Research Objects. In this study, 50 patients with AIDS and spinal tuberculosis (experimental group) and 50 patients with spinal tumors (control group) in the hospital from February 2, 2020, to June 2, 2021, were selected, with the age range of 20–69 years. This study obtained the informed consent of patients and their families, who had signed the informed consent forms in strict accordance with relevant regulations. This study had been approved by the Ethics Committee of the hospital.

The inclusion criteria were given as follows: patients diagnosed with spinal tuberculosis or spinal tumors by clinical symptoms and laboratory tests; patients diagnosed with AIDS according to the *Guidelines for the Diagnosis and Treatment of AIDS* in China; patients with MRI and CT examinations; and patients without examination contraindications.

The exclusion criteria were described as follows: patients who were critically ill; patients whose image quality was too poor; patients with mental illness and could not cooperate with surgical treatment; and patients whose family members did not agree and did not sign informed consent.

2.2. MRI and CT Imaging Examination. CT and MRI imaging examinations were performed on 100 patients. The scanning position included the patient's diseased cone and adjacent cones. The examination conditions were set according to Table 1.

A 1.5-T magnetic MRI system was used to scan from three positions, namely, the transverse position, the coronal position, and the sagittal position. The thickness of the transverse scan was 3.6 mm, and the thickness of the other two azimuths was 3 mm. The layer spacing was 1 mm, the field of view (FOV) was between 200 mm and 340 mm, and the matrix was 256×256.

2.3. Improved Inception-ResNet Classification Algorithm. The residual structure appears in the ResNet model, which makes it easier to optimize. In the propagation process of neural networks, the backpropagation often causes the propagation gradient to gradually disappear during the propagation process, which can be solved due to the existence of the residual structure. The gradient information of

Table 1: Scan conditions of the CT imaging test.

Conditions	Current (mAs)	Voltage (kV)	Effective layer thickness (mm)	Pitch
Value	200–270	90–125	5	1–1.5

the residual structure is easier to propagate during the backpropagation process, and the network with the residual module will also get a higher recognition accuracy. At the same time, the ResNet residual network model uses a large batch of relatively standardized methods for enzyme training, and its specific structure model is shown in Figure 1.

The network structure models of ResNet and Inception were combined, while the SE-block and stem were introduced to form a new network structure with many advantages. First, the size of the convolution kernel was changed. In order to increase the speed of operation and deepen the network depth, the original convolution kernel of the Inception structure was decomposed from 5×5 and 7×7 into 5×1 and 1×5 and 7×1 and 1×7. Second, the ResNet residual structure was combined with the Inception model to avoid the disappearance of gradient information in the backpropagation process. At the same time, the addition of SE-block changed the existing activation function of the change itself to LeakyReLU, which enhanced the network characteristics and realized the improvement of the network generalization function.

The model idea of ResNet-Inception was described as follows: first, it should extract the feature information in the Inception network picture and output the read result a, thereby completing the global average pooling. Second, the result obtained in the previous step was allowed to pass through the fully connected layer, so that the updated result was $B_1 \times a$ to reduce the number of channels in the result a and reduce the calculation parameters. Third, the values were continually assigned via the activation function of the nonlinear layer, and the result of the activation function was outputted, which was denoted as C. Fourth, the result was successively input to the fully connected layer, another parameter D was introduced, and the result $D_2C\,(B_1 \times a)$ was outputted, so as to achieve the goal of reducing the number of channels. Next, the result obtained in the previous step was delivered to the nonlinear layer, and then, the weight data of each channel mentioned above were obtained. Finally, the collection of all information parameters was realized in the fully connected layer. At the end of this model, the corresponding information of the two models (ResNet and Inception) was superimposed. The residual module belonging to ResNet was only combined with Inception in the last step. The function equation was given as follows:

$$N = R\left(D_2C\left(B_1 \times a\right)\right). \tag{1}$$

In the classification algorithm of this study, cross entropy was also introduced as a loss function, where c and d were two standardized probability distributions, and the cross entropy of c was represented by d (as shown in (2)) as follows:

$$M(c, d) = -\sum c(a)\log\, d(a). \tag{2}$$

As shown in equations (3) and (4) below, the cross entropy had to satisfy the probability distribution function as follows:

$$\forall ac\,(X - a) \in [0, 1], \tag{3}$$

$$\sum c\,(X - a) = 1. \tag{4}$$

2.4. Evaluation Criteria. In this study, three common indicators were used to evaluate the diagnostic effect of AIDS combined with spinal tuberculosis using MRI combined with CT based on improved algorithms. They were accuracy, specificity, and sensitivity. The calculation methods were as follows:

$$\text{accuracy} = \frac{A + B}{A + C + B + D}, \tag{5}$$

$$\text{specificity} = \frac{B}{C + B}, \tag{6}$$

$$\text{sensitivity} = \frac{A}{D + A}. \tag{7}$$

Here, A is true positive, which meant that the diagnosis result was positive but the actual result was positive; B refers to true negative, which meant the diagnosis result was negative but the actual result was negative; C is false positive, which meant that the diagnosis result was positive but the actual result was negative; D represents false negative, which meant that the actual result was positive and the diagnosis result was negative.

In this study, the traditional ResNet18 and GoogLeNet were introduced and compared with the improved Inception-ResNet classification algorithm for further comparison and analysis.

2.5. Construction of the Experimental Environment. The experimental environment of this study was as follows: central processing unit (CPU), Intel I7-7700; graphics processing unit (GPU), Nvidia RTX2070; Windows 10 operating system, and Python language (PyTorch and conda).

2.6. Statistical Analysis. The SPSS software was applied to statistically analyze the data. Data that conformed to normal distribution were represented by mean ± standard deviation ($x \pm s$), the t-test was used to represent measurement data, and the chi-square (χ^2) test was used to represent count data. $P < 0.05$ indicated statistical difference.

3. Results

3.1. Diagnostic Results of MRI Combined with CT Based on Improved Algorithm. The accuracy, specificity, and sensitivity of the algorithms were calculated and compared. The

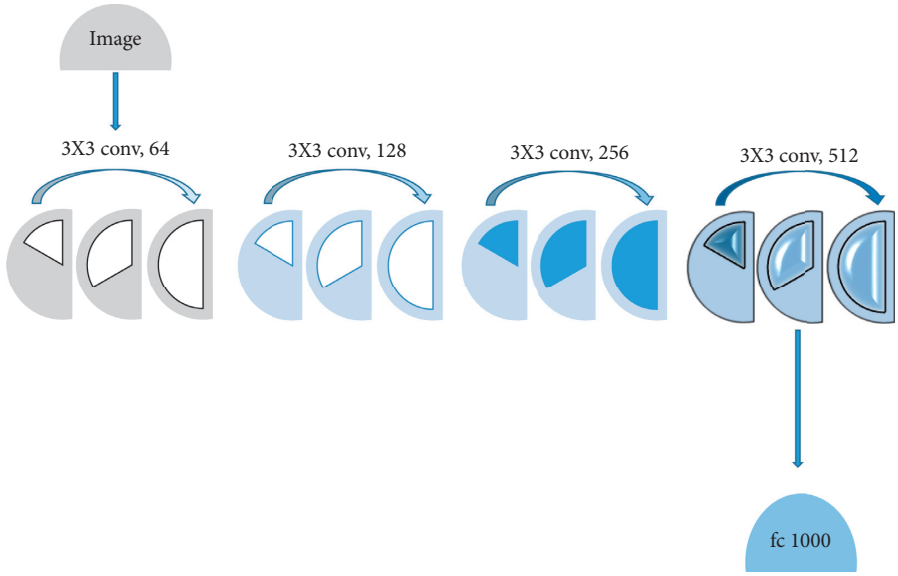

Figure 1: Schematic diagram for structure model of ResNet.

accuracy, specificity, and sensitivity of the Inception-ResNet classification algorithm were 96.7%, 98.4%, and 96.3%, respectively; those of the GoogLeNet algorithm were 94.9%, 97.9%, and 93.9%, respectively; and those of the ResNet algorithm were 94.7%, 96.7%, and 94.9%, respectively. In addition, it was found that the accuracy, specificity, and sensitivity of the Inception-ResNet classification algorithm were significantly higher than those of ResNet18 and GoogLeNet ($P < 0.05$). The specific results are shown in Figures 2–4.

3.2. The Result of the Loss Function of the Improved Algorithm. After comparison on training loss functions of the three algorithms, it was found that the loss function of the Inception-ResNet classification algorithm had reached convergence after 350 times, and the training loss of ResNet and GoogLeNet algorithms had reached convergence after 700 times. The specific results are shown in Figure 5.

At the same time, the training time and parameter amount of the three algorithms were compared and analyzed, and it was found that the training time and parameter amount of the Inception-ResNet algorithm were greatly lower than those of the other two algorithms ($P < 0.05$). The specific results are shown in Figure 6.

3.3. MRI and CT Imaging Data of AIDS Patients with Spinal Tuberculosis. Figure 7 shows the images of a patient, who was a 35-year-old male with a history of Horner's syndrome, and his neck was enlarged. CT and MRI imaging examinations were performed after admission. The results of CT examinations showed that a large number of pyramidal bone worm-like damages spread all over the upper thoracic spine, and a huge low-density edge-enhancing cold abscess was formed in front of the pyramid. The results of the MRI examination were relatively consistent with CT. In addition to pyramidal lesions, damage to surrounding soft tissues can also be observed.

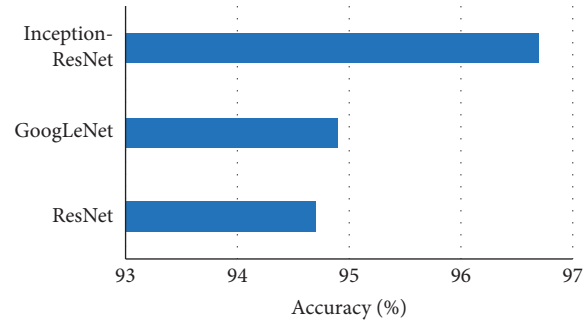

Figure 2: Comparison of accuracy of three algorithms. Note: *the difference was statistically great ($P < 0.05$).

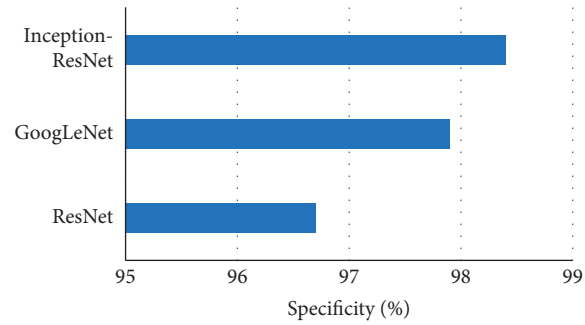

Figure 3: Comparison of specificity of three algorithms. Note: *the difference was statistically great ($P < 0.05$).

3.4. Comparison of Misdiagnosis Rates of Different Algorithms for AIDS Combined with Spinal Tuberculosis. The misdiagnosis rate of AIDS combined with spinal tuberculosis under three different algorithms was calculated and compared. It was found that the improved ResNet-Inception algorithm showed a misjudgment rate of about 4%, which was lower than that of the ResNet18 and GoogLeNet algorithms, and the differences were statistically obvious ($P < 0.05$). The specific results are shown in Figure 8.

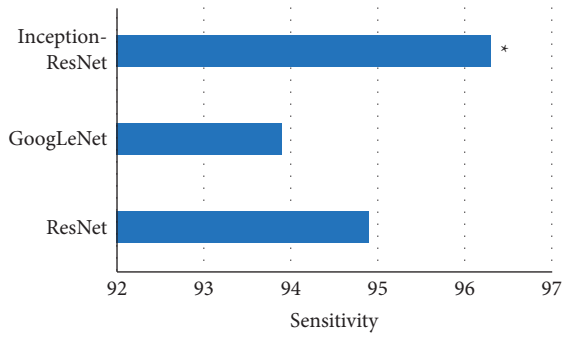

Figure 4: Comparison of sensitivity of three algorithms. Note: *the difference was statistically great ($P < 0.05$).

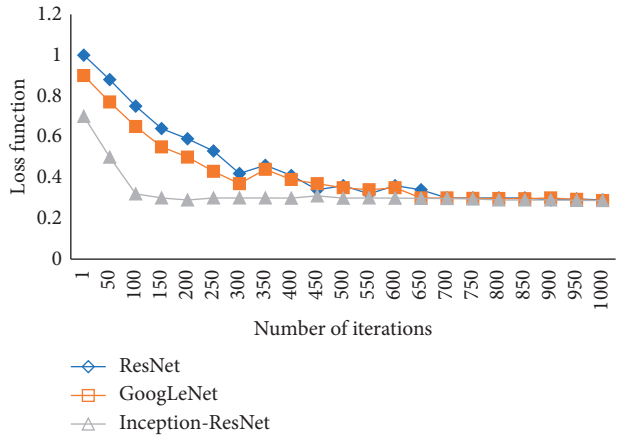

Figure 5: Loss functions of the three algorithm models.

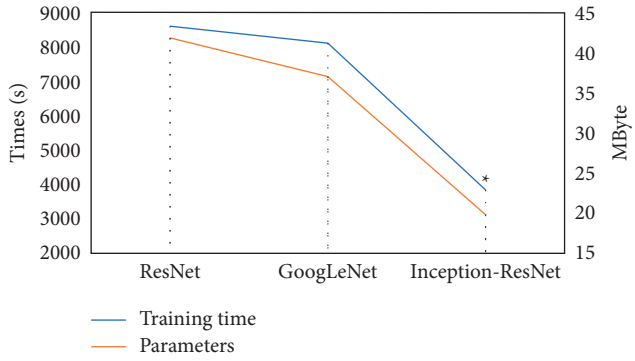

Figure 6: Comparison of training time and parameter amount of the three algorithms. Note: *the difference was statistically great ($P < 0.05$).

4. Discussion

At present, the morbidity and mortality of AIDS combined with spinal tuberculosis are gradually increasing. One-third of AIDS patients worldwide die from spinal tuberculosis, and tuberculosis has surpassed AIDS to become the infectious disease with the most death pathology in the world. The dual infection of AIDS and tuberculosis is a process of mutual exacerbation of the disease process, which leads to rapid death. The death rate of AIDS combined with spinal tuberculosis is as high as 80%. Therefore, the accurate diagnosis and examination of the disease are extremely important [25, 26]. In this study, an improved algorithm was proposed based on MRI combined with CT to diagnose and check AIDS combined with spinal tuberculosis. This improved algorithm combined the ResNet and Inception network structures as well as the stem, SE-block, and reduction to form an improved CNGC. The results showed that the accuracy, specificity, and sensitivity of the Inception-ResNet classification algorithm were 96.7%, 98.4%, and 96.3%, respectively; those of the GoogLeNet algorithm were 94.9%, 97.9%, and 93.9%, respectively; and those of the ResNet algorithm were 94.7%, 96.7%, and 94.9%, respectively. Compared with the traditional ResNet18 and GoogLeNet, it was found that the accuracy, specificity, and sensitivity of the improved ResNet-Inception algorithm were significantly higher than those of the ResNet18 and GoogLeNet algorithms. In addition, compared with the training loss of ResNet18 and GoogLeNet algorithms that converge after 700 times, the ResNet-Inception algorithm only required 350 times to achieve convergence. This showed that the improved ResNet-Inception algorithm was more valuable than the traditional ResNet18 and GoogLeNet algorithms for MRI combined with CT diagnosis of AIDS combined with spinal tuberculosis.

In this study, 50 AIDS patients with spinal tuberculosis and 50 patients with spinal tumors were selected as the research objects for MRI and CT imaging examinations. The diagnostic effect of MRI combined with CT on AIDS combined with spinal tuberculosis under different algorithms was compared. Spinal tumors and AIDS combined with spinal tuberculosis are two common diseases in spinal surgery that are difficult to differentiate and diagnose. The clinical symptoms are mostly low back pain, radiating pain, low-grade fever, chills, anorexia, weight loss, and other nonspecific symptoms. Even if there may be symptoms of the primary lesion, it cannot be said that spinal lesions are secondary lesions. Tumor metastasis or extrapulmonary tuberculosis requires definite evidence, and the specialty signs are mostly positive signs of spinal destruction, loss of spinal stability, and involvement of soft tissues such as periosteum, nerve roots, and paravertebral muscles [27, 28]. Spine surgeons often judge the difference between the two typical imaging findings before surgery. The lesions invade and destroy the intervertebral space and often have paravertebral abscesses and spinal tuberculosis; if the lesion invades along the pedicle, it is roughly judged to be spinal tumors [29]. Excellent improved algorithms are essential in this judgment process. The results of this study showed that the imaging examination based on the improved ResNet-Inception algorithm had a misdiagnosis rate of only 4% for AIDS combined with spinal tuberculosis, which was significantly lower than the other two traditional algorithms ($P < 0.05$), and the differential diagnosis of tumors showed great clinical value. Boruah et al. (2021) [30] retrospectively evaluated the MRI imaging data of 19 patients with spinal tuberculosis and found that it was very important for the early diagnosis of patients, which was beneficial to reduce the morbidity and severity of patients. Another study

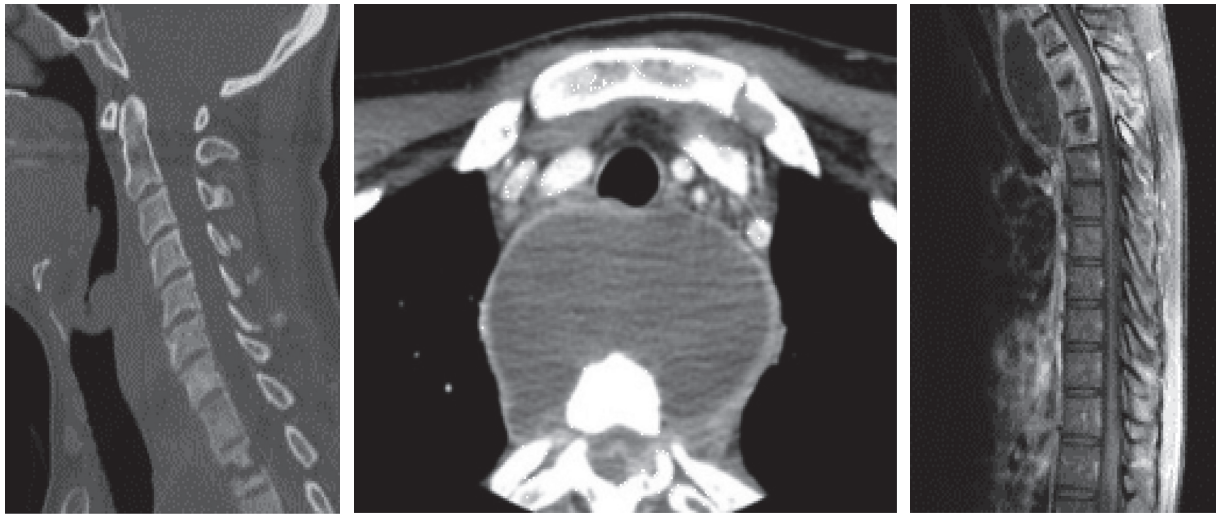

Figure 7: MRI and CT imaging examinations of AIDS patients with spinal tuberculosis.

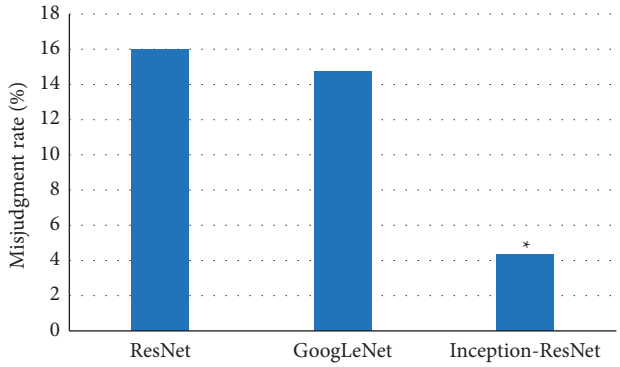

Figure 8: Misdiagnosis rates of different algorithms for AIDS combined with spinal tuberculosis. Note: *the difference was statistically great ($P < 0.05$).

retrospectively analyzed the MRI and CT imaging features of spinal tuberculosis and tumors and found that it can be used in the differential diagnosis of spinal tuberculosis and spinal tumors [31], which is consistent with the conclusions of this study. However, spinal tuberculosis and tumors have different manifestations at different stages of disease progression, and special cases may have atypical manifestations. Tumors may also destroy the intervertebral space, and tuberculosis does not necessarily destroy the pedicle. The diagnosis of any disease needs to be combined with clinical symptoms, signs, laboratory, and imaging examinations. Therefore, the further diagnosis of AIDS combined with spinal tuberculosis requires histopathological results as the gold standard.

5. Conclusion

The improved algorithm was applied to AIDS patients with spinal tuberculosis and compared with the traditional ResNet18 and GoogLeNet to evaluate its diagnostic effect and value. 50 patients with AIDS and spinal tuberculosis and 50 patients with spinal tumors were selected for MRI and CT scans. The diagnostic effects of different classification algorithms on AIDS combined with spinal tuberculosis were compared, and it was found that the improved ResNet-Inception algorithm effectively improves the accuracy, specificity, and sensitivity of imaging diagnosis of AIDS combined with spinal tuberculosis. The identification effect of AIDS combined with spinal tuberculosis was stronger than the other two traditional algorithms, and the improved algorithm can be applied to clinical imaging diagnosis. This study provided an effective clinical basis for the diagnosis of AIDS complicated with spinal tuberculosis and offered a great reference value for the differential diagnosis of AIDS and spinal tumors. The shortcomings of this study were that the sample size of the research objects was small, and the source was single, which did not have randomness and wide applicability. Insubsequent studies, analysis, and research of multiple locations and multiple types, large sample sizes would be considered to provide a more practical and effective reference value for imaging examination and diagnosis of AIDS combined with spinal tuberculosis.

Data Availability

The data used to support the findings of this study are available from the corresponding author upon request.

Conflicts of Interest

The authors declare no conflicts of interest.

References

[1] T. C. Quinn, "Forty years of AIDS: a retrospective and the way forward," *Journal of Clinical Investigation*, vol. 131, no. 18, Article ID e154196, 2021.

[2] D. B. Meya, L. Tugume, V. Nabitaka et al., "Establishing targets for advanced HIV disease: a call to action," *Southern African Journal of HIV Medicine*, vol. 22, no. 1, p. 1266, 2021.

[3] Z. Wan, Y. Dong, Z. Yu, H. Lv, and Z. Lv, "Semi-supervised support vector machine for digital twins based brain image fusion," *Frontiers in Neuroscience*, vol. 15, Article ID 705323, 2021.

[4] S. Momenyan, "Joint analysis of longitudinal measurements and spatially clustered competing risks HIV/AIDS data," *Statistics in Medicine*, vol. 40, no. 28, pp. 6459–6477, 2021.

[5] C. Kakalou, E. Polychronidou, V. Drosou et al., "RiskRadar: development and pilot results of a technical intervention targeting combination prevention regarding HIV, viral hepatitis, sexually transmitted infections and tuberculosis," *BMC Infectious Diseases*, vol. 21, no. Suppl 2, p. 866, 20213.

[6] C. Anterasian, A. J. Warr, S. M. Lacourse et al., "Non-ifnγ whole blood cytokine responses to Mycobacterium tuberculosis antigens in HIV-exposed infants," *The Pediatric Infectious Disease Journal*, vol. 40, no. 10, pp. 922–929, 2021.

[7] A. Uppal, S. Rahman, J. R. Campbell, O. Oxlade, and D. Menzies, "Economic and modeling evidence for tuberculosis preventive therapy among people living with HIV: A systematic review and meta-analysis," *PLoS Medicine*, vol. 18, no. 9, Article ID e1003712, 2021.

[8] A. M. Al-Hayani, S. A. Kamel, S. S. Almudarra, M. Alhayani, and A. Abu-Zaid, "Drug resistance to anti-tuberculosis drugs: a cross-sectional study from makkah, Saudi Arabia," *Cureus*, vol. 13, no. 8, Article ID e17069, 2021.

[9] S. Bae, Y.-J. Kim, M.-J. Kim et al., "Risk of tuberculosis in patients with cancer treated with immune checkpoint inhibitors: a nationwide observational study," *Journal for ImmunoTherapy of Cancer*, vol. 9, no. 9, Article ID e002960, 2021.

[10] O. Oxlade, H. Rochon, J. R. Campbell, and D. Menzies, "Tuberculosis preventive treatment in people living with HIV-Is the glass half empty or half full?" *PLoS Medicine*, vol. 18, no. 9, Article ID e1003702, 2021.

[11] R. Bhosale, M. Alexander, P. Deshpande et al., "Stages of pregnancy and HIV affect diagnosis of tuberculosis infection and Mycobacterium tuberculosis (MTB)-induced immune response: findings from PRACHITi, a cohort study in Pune, India," *International Journal of Infectious Diseases*, vol. 112, no. 21, pp. 205–211, 2021.

[12] P. MacPherson, E. L. Webb, W. Kamchedzera et al., "Computer-aided X-ray screening for tuberculosis and HIV testing among adults with cough in Malawi (the PROSPECT study): a randomised trial and cost-effectiveness analysis," *PLoS Medicine*, vol. 18, no. 9, Article ID e1003752, 2021.

[13] P. Rajpurkar, C. O'Connell, A. Schechter et al., "CheXaid: deep learning assistance for physician diagnosis of tuberculosis using chest x-rays in patients with HIV," *Npj Digital Medicine*, vol. 3, no. 1, p. 115, 2020.

[14] A. Mukhatayeva, A. Mustafa, N. Dzissyuk et al., "Hepatitis B, Hepatitis C, tuberculosis and sexually-transmitted infections among HIV positive patients in Kazakhstan," *Scientific Reports*, vol. 11, no. 1, p. 18123, 2021.

[15] A. F. Auld, A. D. Kerkhoff, Y. Hanifa et al., "Derivation and external validation of a risk score for predicting HIV-associated tuberculosis to support case finding and preventive therapy scale-up: a cohort study," *PLoS Medicine*, vol. 18, no. 9, Article ID e1003739, 2021.

[16] M. R. Ticlla, J. Hella, H. Hiza et al., "The sputum microbiome in pulmonary tuberculosis and its association with disease manifestations: A cross-sectional study," *Frontiers in Microbiology*, vol. 12, Article ID 633396, 2021.

[17] M. Ihsan Mutt, F. Stephanie, M. Saragih, and U. S. Friend Tam, "Epitope-based vaccine design for tuberculosis HIV infection through in silico approach," *Pakistan Journal of Biological Sciences*, vol. 24, no. 7, pp. 765–772, 2021.

[18] Y. Li, J. Zhao, Z. Lv, and J. Li, "Medical image fusion method by deep learning," *International Journal of Cognitive Computing in Engineering*, vol. 2, no. 6, pp. 21–29, 2021.

[19] L. Nakiyingi, J. M. Bwanika, W. Ssengooba et al., "Chest X-ray interpretation does not complement Xpert MTB/RIF in diagnosis of smear-negative pulmonary tuberculosis among TB-HIV co-infected adults in a resource-limited setting," *BMC Infectious Diseases*, vol. 21, no. 1, p. 63, 2021.

[20] D. Li, W. He, B. Chen, and P. Lv, "Primary multidrug-resistant tuberculosis versus drug-sensitive tuberculosis in non-HIV-infected patients: comparisons of CT findings," *PLoS One*, vol. 12, no. 6, Article ID e0176354, 2017.

[21] A. Di Napoli, M. Cristofaro, A. Romano et al., "Central nervous system involvement in tuberculosis: an MRI study considering differences between patients with and without Human Immunodeficiency Virus 1 infection," *Journal of Neuroradiology*, vol. 47, no. 5, pp. 334–338, 2020.

[22] S. Xie, Z. Yu, and Z. Lv, "Multi-disease prediction based on deep learning: a survey," *Computer Modeling in Engineering and Sciences*, vol. 128, no. 2, pp. 489–522, 2021.

[23] D. Chen, P. Wawrzynski, and Z. Lv, "Cyber security in smart cities: a review of deep learning-based applications and case studies," *Sustainable Cities and Society*, vol. 66, Article ID 102655, 2021.

[24] A. D. Grant, S. Charalambous, M. Tlali et al., "Algorithm-guided empirical tuberculosis treatment for people with advanced HIV (TB Fast Track): an open-label, cluster-randomised trial," *The Lancet HIV*, vol. 7, no. 1, pp. e27–e37, 2020.

[25] P. Y. Khan, T. A. Yates, M. Osman et al., "Transmission of drug-resistant tuberculosis in HIV-endemic settings," *The Lancet Infectious Diseases*, vol. 19, no. 3, pp. e77–e88, 2019.

[26] S. C. Auld and B. S. Staitieh, "HIV and the tuberculosis "set point": how HIV impairs alveolar macrophage responses to tuberculosis and sets the stage for progressive disease," *Retrovirology*, vol. 17, no. 1, p. 32, 2020.

[27] T. V. Stepanova, O. P. Nedospasova, and M. V. Golubchykov, "Analysis of tuberculosis/hiv co-infection trends in Ukraine in 2008-2017," *Wiadomosci Lekarskie*, vol. 72, no. 5 cz 1, pp. 903–907, 2019.

[28] W. N. Phoswa, S. Eche, and O. P. Khaliq, "The association of tuberculosis mono-infection and tuberculosis-Human immunodeficiency virus (TB-HIV) Co-infection in the pathogenesis of hypertensive disorders of pregnancy," *Current Hypertension Reports*, vol. 22, no. 12, p. 104, 2020.

[29] F. E. Ejeh, A. Undiandeye, K. Okon, H. M. Kazeem, and A. C. Kudi, "Isolation and immunological detection of Mycobacterium tuberculosis from HIV and non-HIV patients in benue state, Nigeria," *Ethiopian Journal of Health Sciences*, vol. 30, no. 1, pp. 55–64, 2020.

[30] D. K. Boruah, B. B. Gogoi, A. Prakash, N. R. Lal, K. Hazarika, and K. K. Borah, "Magnetic resonance imaging evaluation of posterior spinal tuberculosis: a cross-sectional study," *Acta Radiologica*, vol. 62, no. 8, pp. 1035–1044, 2021.

[31] J. Białecki, M. Nowak-Misiak, K. Rąpała, W. Marczyński, G. Suchodolski, and A. Truszczyńska, "Spinal tuberculosis with severe neurological symptoms as a complication of intravesical BCG therapy for carcinoma of the bladder," *Neurologia I Neurochirurgia Polska*, vol. 50, no. 2, pp. 131–138, 2016.